



The impacts of phosphorus deficiency on the photosynthetic electron transport chain

Carstensen, Andreas; Herdean, Andrei; Schmidt, Sidsel Birkelund; Sharma, Anurag; Spetea, Cornelia; Pribil, Mathias; Husted, Søren

Published in:
Plant Physiology

DOI:
[10.1104/pp.17.01624](https://doi.org/10.1104/pp.17.01624)

Publication date:
2018

Document version
Publisher's PDF, also known as Version of record

Citation for published version (APA):
Carstensen, A., Herdean, A., Schmidt, S. B., Sharma, A., Spetea, C., Pribil, M., & Husted, S. (2018). The impacts of phosphorus deficiency on the photosynthetic electron transport chain. *Plant Physiology*, 177, 271-284. <https://doi.org/10.1104/pp.17.01624>

The Impacts of Phosphorus Deficiency on the Photosynthetic Electron Transport Chain¹[OPEN]

Andreas Carstensen,^a Andrei Herdean,^b Sidsel Birkelund Schmidt,^a Anurag Sharma,^a Cornelia Spetea,^b Mathias Pribil,^a and Søren Husted^{a,2}

^aCopenhagen Plant Science Centre, Department of Plant and Environmental Sciences, Faculty of Science, University of Copenhagen, 1871 Frederiksberg C, Denmark

^bDepartment of Biological and Environmental Sciences, University of Gothenburg, Gothenburg 405 30, Sweden

ORCID IDs: 0000-0001-5029-7015 (A.C.); 0000-0003-2143-0213 (A.H.); 0000-0002-4193-4454 (S.B.S.); 0000-0001-5345-8830 (A.S.); 0000-0001-7609-0290 (C.S.); 0000-0002-9174-9548 (M.P.); 0000-0003-2020-1902 (S.H.).

Phosphorus (P) is an essential macronutrient, and P deficiency limits plant productivity. Recent work showed that P deficiency affects electron transport to photosystem I (PSI), but the underlying mechanisms are unknown. Here, we present a comprehensive biological model describing how P deficiency disrupts the photosynthetic machinery and the electron transport chain through a series of sequential events in barley (*Hordeum vulgare*). P deficiency reduces the orthophosphate concentration in the chloroplast stroma to levels that inhibit ATP synthase activity. Consequently, protons accumulate in the thylakoids and cause lumen acidification, which inhibits linear electron flow. Limited plastoquinol oxidation retards electron transport to the cytochrome *b₆f* complex, yet the electron transfer rate of PSI is increased under steady-state growth light and is limited under high-light conditions. Under P deficiency, the enhanced electron flow through PSI increases the levels of NADPH, whereas ATP production remains restricted and, hence, reduces CO₂ fixation. In parallel, lumen acidification activates the energy-dependent quenching component of the nonphotochemical quenching mechanism and prevents the overexcitation of photosystem II and damage to the leaf tissue. Consequently, plants can be severely affected by P deficiency for weeks without displaying any visual leaf symptoms. All of the processes in the photosynthetic machinery influenced by P deficiency appear to be fully reversible and can be restored in less than 60 min after resupply of orthophosphate to the leaf tissue.

Phosphorus (P) is an essential heteroelement in compounds such as ATP, NADPH, nucleic acids, sugar phosphates, and phospholipids, all of which play important roles in photosynthesis (Hammond and White, 2008). Consequently, even marginal P deficiency has a major impact on plant growth and development. It has been estimated that 30% of the world's arable soils are deficient in P and require P fertilization to improve yields (MacDonald et al., 2011). However, phosphate rock, the source of mineral P fertilizers, is a finite natural resource, and known reserves are projected to last

less than a few hundred years at current rates of consumption (Cordell et al., 2009; Gilbert, 2009; Walan et al., 2014; Baker et al., 2015). This makes P a strategic natural resource similar to oil, as a few countries control most known reserves. Currently, some parts of the world vastly overuse P fertilization, which causes eutrophication of lakes and coastal waters, whereas limited access to P fertilizer causes crop yield reductions elsewhere (Baker et al., 2015). P fertilizer is rapidly immobilized in the soil due to chemical fixation and microbial immobilization; therefore, excessive P application often is required to ensure ample P availability to plants. As a result, less than 20% of P fertilizer added to soils is typically taken up by the crop (Cordell and White, 2015). This obviously low P use efficiency is unsustainable.

Orthophosphate (P_i) is a major regulator of carbon metabolism in plants, and P deficiency influences the balance between the synthesis and catabolism of carbon metabolites. Low P_i levels switch the carbon flow to starch accumulation and reduce CO₂ assimilation (Heldt et al., 1977). Plants have evolved several responses to balance and stabilize the fluctuating P_i levels that occur at the tissue level in natural environments, such as (1) altering root morphology and initiating mycorrhizal symbiosis to improve soil exploration for P; (2) activating exudation processes in the rhizosphere to mobilize P_i from the soil; (3) inducing P_i transporter

¹ This work was supported by the University of Copenhagen and Innovation Fund Denmark (Future Cropping). A.H. was the recipient of a postdoctoral fellowship from the Foundation Olle Engkvist Byggmästare, and A.S. would like to thank Carlsbergfondet for support.

² Address correspondence to shu@plen.ku.dk.

The author responsible for distribution of materials integral to the findings presented in this article in accordance with the policy described in the Instructions for Authors (www.plantphysiol.org) is: Søren Husted (shu@plen.ku.dk).

A.C., A.H., A.S., C.S., M.P., and S.H. designed the experiments; A.C. and A.H. performed the fluorescence measurements; A.C. and S.B.S. performed the enzyme assays, including the immunoblot analyses; A.S. performed the transmission electron microscopy; all authors participated in data interpretation; A.C. and S.H. drafted the article, and all authors participated in completing the final version.

[OPEN] Articles can be viewed without a subscription.

www.plantphysiol.org/cgi/doi/10.1104/pp.17.01624


Treatment	P ($\mu\text{g g}^{-1}$ DW)	Youngest fully-expanded leaves (28 DAP)
Control	4,400 ^a \pm 366	
P deficient	852 ^b \pm 91	
P resupply	5,026 ^a \pm 624	

Figure 1. Leaf P concentrations with corresponding photographs of the youngest fully expanded barley leaves. Control, P-deficient, and P-resupplied barley plants were cultivated in hydroponics. P was resupplied to the nutrient solution 21 DAP, and each photograph was taken before harvest 7 d later (28 DAP). The P concentrations are mean values in leaf dry matter \pm SE ($n = 4$, each with four technical replicates), and different letters represent statistically significant changes ($P < 0.05$) using one-way ANOVA and Tukey's multiple comparison test. DW, Dry weight.

proteins and regulating P_i uptake kinetics; and (4) remobilizing P_i in source organs to meet the requirements of the developing sink tissue (Ramaekers et al., 2010). These responses are supported by homeostatic processes at the cellular level, in which P_i levels are stabilized by mobilization between storage pools in vacuoles and other organelles such as chloroplasts where the photosynthetic machinery is located (Zhang et al., 2014).

Homeostatic P_i levels in chloroplasts are controlled by a range of different P_i transporters, which are located in the chloroplast inner envelope or in the thylakoid membrane (Młodzińska and Zboińska, 2016). Three classes of chloroplast P_i transporters have been cloned and characterized: the PHT2, PHT4, and plastidic P_i translocators. The high-affinity P_i transporter PHT4;1 ($K_m < 400 \mu\text{M}$) has been localized in the stroma-exposed regions of the thylakoid membrane and mediates P_i transport from the thylakoid lumen to the stroma (Guo et al., 2008; Pavón et al., 2008; Yin et al., 2015). A study of *Arabidopsis* (*Arabidopsis thaliana*) knockout mutants showed that the absence of PHT4;1 resulted in a marked decrease in ATP synthase activity; it was assumed that PHT4;1 operates in close proximity to ATP synthase in the thylakoid membrane to maintain sufficient P_i levels for ATP synthesis (Karlsson et al., 2015). It was proposed that an altered supply of P_i in the stroma reduced the ATP levels and, thereby, reduced CO_2 assimilation, but no changes in the photosynthetic machinery composition or electron transport activity were observed (Karlsson et al., 2015). P starvation immediately affects CO_2 assimilation but does not appear to terminate it, as P-deficient plants typically remain green and do not develop leaf chlorosis. Specifically, P deficiency is believed to affect CO_2 assimilation by reducing the ATP-dependent regeneration of ribulose-1,5-bisphosphate in the Calvin cycle (Rao and Terry, 1995; Yan et al., 2015), whereas its effects on the amounts and carboxylation activity of Rubisco are less clear (Rychter and Rao, 2005; Reich et al., 2009; Muneer and Jeong, 2015).

We recently showed that even marginal P deficiency has a marked effect on electron transport

between PSII and PSI (Frydenvang et al., 2015). An analysis of chlorophyll *a* fluorescence (OJIP) transients indicated that the I-step in the electron transport chain was markedly affected by P deficiency and that the change in the fluorescence transient curvature could be used to quantify the bioactive pool of P_i in plants. However, the targets of P deficiency within the thylakoids upstream of ATP synthase remain largely unknown despite decades of research. The objective of this study was to develop a comprehensive biological model of how photosynthesis is affected by P deficiency under physiologically relevant conditions.

RESULTS

Plant Growth under P Deficiency

Multiple sets of barley plants (*Hordeum vulgare* 'Quench') were hydroponically cultivated using three different treatments: (1) the control treatment, in which plants were treated with a sufficient nutrient supply throughout the experiment; (2) the P-deficient treatment, in which plants were treated with all nutrients as in the control treatment but with a restricted (low) P concentration; and (3) the P-resupply treatment, in which P-deficient plants were supplemented with P concentrations similar to those used in the control treatment at 21 or 25 d after planting (DAP). The plant material was harvested at 28 DAP. P deficiency was observed to reduce plant tillering and biomass, whereas it increased anthocyanin accumulation in stems (Supplemental Fig. S1). The three different treatments resulted in leaf tissue P concentrations ranging from less than $1,000 \mu\text{g P g}^{-1}$ dry weight for P deficiency (treatment 2) to more than $4,000 \mu\text{g P g}^{-1}$ dry weight in the youngest fully expanded leaves (YFELs) for the control (treatment 1) and P resupply (treatment 3; Fig. 1). We confirmed that the plants had no nutrient deficiencies other than P (Supplemental Table S1). Despite the large range of leaf P concentrations, no visual differences between leaves were observed.

Chlorophyll *a* Fluorescence Measurements Revealed P Deficiency

Chlorophyll *a* fluorescence transients (OJIP transients) from the three different treatments revealed a depletion of the I-step for the P-deficient plants (Fig. 2A). Before P resupply at 21 DAP in treatment 3, plants subjected to control and P-deficient treatments were easily differentiated when focusing on the I-step. Seven days after P resupply to P-deficient plants (28 DAP), the I-step returned to control conditions, and the flat plateau resembling the I-step was even more distinct than that observed for the control plants (Fig. 2A, inset). To demonstrate that P deficiency in plants is highly reversible and that disruptions in electron transport can be recovered rapidly, we infiltrated P-deficient leaf segments with a P_i-containing solution by immersion for 60 min. The I-step of the OJIP transients in P-deficient plants was highly reversible and displayed a response to P infiltration into leaves in less than 1 h (Fig. 2B). The quantum efficiency of PSII (F_v/F_m) was unable to discriminate between the treatments because all transients reached values close to the theoretical maximum of 0.83. The fluorescence quenching kinetics after reaching the maximum fluorescence (Fig. 2A, P-step) was much faster for the P-deficient plants than for the control and P-resupplied plants. The slopes of the fluorescence quenching curves between 2 and 10 s were -0.035 ± 0.001 , -0.066 ± 0.002 , and -0.04 ± 0.002 for the control, P-deficient, and P-resupplied plants, respectively. These results indicated that fluorescence quenching in plants resupplied with P did not differ significantly from that of control plants. Therefore, changes in both the I-step and the fluorescence quenching kinetics appear to be highly valuable for diagnosing P deficiency.

Inhibition of Electron Transport to PSI Depletes the I-Step in the Fluorescence Transient

Chemical inhibitors are commonly used to study electron flow in photosynthesis. We used three different inhibitors to manipulate electron transfer in the YFELs of control plants (Fig. 3A). Leaves infiltrated with 3-(3,4-dichlorophenyl)-1,1-dimethylurea (DCMU) exhibited chlorophyll *a* fluorescence transients that lacked both the J- and I-steps (Fig. 3A). DCMU displaces the quinone acceptor Q_B from its binding site, thereby blocking any further electron transfer downstream of PSII by preventing Q_A⁻ reoxidation (Duysens and Sweers, 1963). Leaves infiltrated with dibromothymoquinone (DBMIB) exhibited transients that lacked the I-step (Fig. 3A), similar to those of P-deficient plants (Fig. 2A). DBMIB is an artificial quinone that tightly binds to the cytochrome (Cyt) *b₆f* complex, thereby preventing plastoquinol (PQH₂) reoxidation (Schansker et al., 2005) and preventing electron transport from PQH₂ to PSI. Leaves infiltrated with methyl viologen (MV) exhibited distinct transients that lacked the I-step (Fig. 3A). When illuminating leaves that

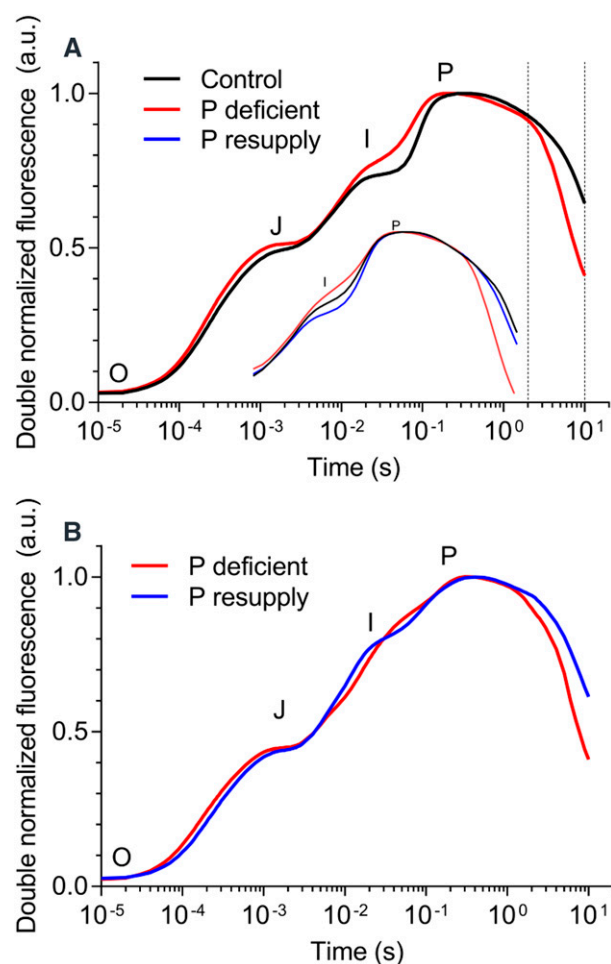


Figure 2. OJIP transients recorded from the youngest, fully expanded barley leaves. A, Main plot. Transients were recorded just before P resupply at 21 DAP. The inset shows transients recorded 7 d after P resupply at 28 DAP. The slope of the quenching curve was calculated between the two dashed vertical lines (between 2 and 10 s). B, Transients recorded for P-deficient leaves immersed in Milli-Q water (P deficient) or P solution (P resupply) for 60 min. All transients were averaged (A, $n = 5$; B, $n = 4$, each with more than four technical replicates) and doubled normalized between F_0 and F_m . A.U., Arbitrary units.

have been dark adapted for more than 10 min, there is a transient restriction in electron flow in PSI because ferredoxin-NADP⁺ reductase (FNR) is inactivated. This transient block is thought to be important for the development of the I-step kinetics. MV is an effective electron acceptor that strongly competes with ferredoxin for electrons from the FeS clusters in PSI, thereby bypassing the transient block imposed by FNR during dark adaption (Schansker et al., 2005). All infiltrations with chemical inhibitors were compared with leaves infiltrated with Milli-Q water as a control.

To further demonstrate that fluorescence transients of P-deficient plants lack the I-step due to the inhibition of electron transport to PSI, OJIP transients were obtained from two *Arabidopsis* PSI mutants, *psad1-1* and *psae1-3*, which have pronounced reductions in the

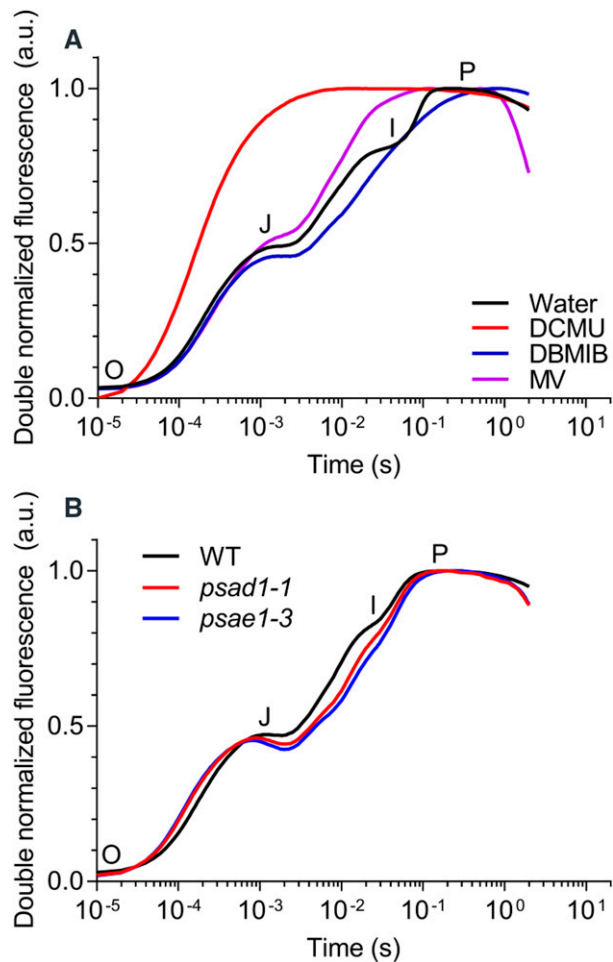


Figure 3. OJIP transients recorded from barley leaves infiltrated with electron inhibitors or from Arabidopsis PSI mutants. A, Effects of DCMU, DBMIB, and MV inhibitors on OJIP transients in the YFELs of 28-d-old healthy barley plants (control) cultivated in hydroponics. B, OJIP transients from 6-week-old Arabidopsis mutants *psad1-1* and *psae1-3* and the corresponding wild type (WT) cultivated in soil. The transients were averaged (A, $n = 4$; B, $n = 5$, each with four technical replicates) and double normalized between F_0 and F_m .

levels of the PSI subunits PsaD1 and PsaE1, respectively. These two mutants have markedly impaired photosynthetic electron flow (Ihnatowicz et al., 2004, 2007). The transients of both mutants essentially lacked the I-step, which is present in wild-type plants (Fig. 3B), which supported the results obtained from experiments with the DCMU, DBMIB, and MV inhibitors (Fig. 3A).

P Deficiency Suppresses the Production of ATP and Increases the Production of NADPH

NADP⁺ is the final substrate for the production of NADPH, and NADPH and ATP are the main products of light-dependent reactions in photosynthesis. The NADP⁺ concentration was reduced significantly in

P-deficient barley plants compared with those in control and P-resupply plants (Fig. 4A). At 3 d after P resupply (28 DAP) to P-deficient plants, the NADP⁺ concentration was restored to that in control plants. The opposite trend was present for NADPH, with the NADPH concentration being significantly higher in P-deficient plants than in control and P-resupplied plants (Fig. 4B). As for the NADP⁺ concentration, the same trend was observed for the ATP concentration in isolated thylakoids, although the ATP level in P-resupplied plants was lower than that in control plants (Fig. 4C). The P_i concentration at the whole-leaf level was reduced severely in the P-deficient plants (Fig. 4D). The total P_i concentration in chloroplasts isolated after either a dark or light period (Fig. 4, E and F, respectively) was significantly lower in the P-deficient plants; however, the relative change was lower than that observed at the whole-leaf level. The starch content was significantly higher in P-deficient plants than in control and P-resupplied plants (Fig. 4G). These differences in starch contents were confirmed visually using transmission electron micrographs of chloroplasts from control, P-deficient, and P-resupplied plants, whereas no striking differences in chloroplast or thylakoid structure were observed (Supplemental Fig. S2).

We further investigated the P-mediated changes in key photosynthetic proteins by performing immunoblot analysis on thylakoids isolated from 28-d-old YFELs using antibodies against FNR, ferredoxin (FDX1), PsaA, PsaF, Cyt_f, D1, and CP43. Visual inspection and quantification of the protein blots confirmed that the different P treatments did not affect the photosynthetic machinery at the protein level (Supplemental Fig. S3; Supplemental Table S2).

A severe reduction in stromal P concentration induced by Man infiltration (Takizawa et al., 2008) or by the absence of the chloroplast-localized P_i transporter PHT4;1 (Karlsson et al., 2015) reduced proton flux through ATP synthase and subsequently induced lumen acidification. To determine if this also occurs in plants subjected to P deficiency at physiologically relevant concentrations, we analyzed the magnitude and partitioning of the proton motive force (*pmf*) that drives ATP synthase. The results showed that P-deficient plants had a reduced ATP synthase activity (Fig. 5A), which is in agreement with the observed reduced ATP concentrations (Fig. 4C). However, 7 d after P resupply (at 28 DAP), ATP synthase activity was fully restored to control levels. Changes in *pmf*, which reflect pH differences across the thylakoid membrane (ΔpH) and differences in the electrical potential ($\Delta\Psi$), were significantly affected by P deficiency (Fig. 5B). The *pmf* in P-deficient plants was essentially determined exclusively by ΔpH (94%), which most probably indicates a highly acidified lumen, whereas the control and P-resupplied plants had *pmf* values reflecting a balanced distribution between ΔpH and $\Delta\Psi$ (Fig. 5B). Since *pmf* size and its components were determined from light-dark measurements of the electrochromic band shift (ECS) signal, the *pmf* size may have been underestimated because the ECS dark relaxation is

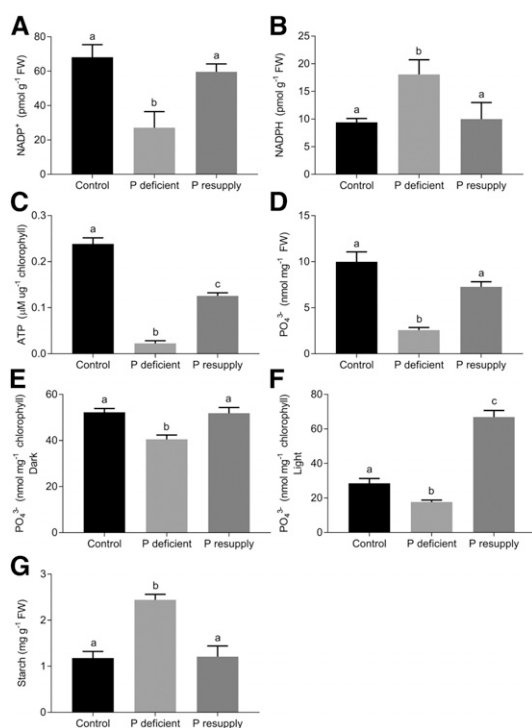


Figure 4. Concentrations of NADP⁺, NADPH, ATP, P_i (PO₄³⁻), and starch in the youngest, fully expanded barley leaves. A, Concentrations of NADP⁺ in leaf tissue. B, Concentrations of NADPH in leaf tissue. C, Concentrations of ATP in light-exposed thylakoids. D, Concentrations of PO₄³⁻ in leaf tissue. E, Concentrations of PO₄³⁻ in chloroplasts isolated after a 10-h dark period. F, Concentrations of PO₄³⁻ in chloroplasts isolated after a 4-h light period. G, Concentrations of starch in leaf tissue. The results are means ± SE (*n* = 4, each with more than four technical replicates), and different letters represent statistically significant changes (*P* < 0.05) using one-way ANOVA and Tukey's multiple comparison test. FW, Fresh weight.

dependent on the free energy for ATP formation, which, in turn, depends on the [ATP]/[ADP]*[P_i] ratio in the chloroplast stroma. However, lumen acidification was further supported by analyzing the extended chlorophyll *a* fluorescence transients (the full OJ-I-PSMT curve; Supplemental Fig. S4). At low saturating actinic light intensity (1,000 μmol photons m⁻² s⁻¹), a distinct disappearance of the S-M phase was observed for P-deficient plants, which was associated previously with lumen acidification and attenuation of the electron flow from PSII to PSI (Goltsev et al., 2016).

Lumen acidification is an immediate signal that triggers the feedback regulation of light capture via the energy-dependent quenching (qE) component, being the largest and most rapidly induced component of nonphotochemical quenching (NPQ; Müller et al., 2001). The NPQ measurements for the three treatments again revealed that P-deficient plants differed from control and P-resupplied plants (Supplemental Fig. S5). NPQ was increased sharply immediately after the onset of illumination in P-deficient plants and was higher than that for control and P-resupplied plants

throughout the entire period of illumination (Supplemental Fig. S5A). Furthermore, NPQ relaxation in the dark was slower for P-deficient plants and associated with a reduction in PSII quantum yield (Supplemental Fig. S5B).

We also directly quantified qE in growth light and at increasing light intensities, which confirmed that this component of NPQ is substantially higher in P-deficient plants across all light intensities (Fig. 6A). Moreover, the electron transfer rate through PSII [ETR(II)] was lower across all light intensities in P-deficient plants (Fig. 6B), whereas the electron transfer rate through PSI [ETR(I)] was higher in growth light and lower with increasing light intensities compared with the control plants (Fig. 6C). Further measurements under steady-state growth light conditions revealed that PSII quantum yield, linear electron flow, and the fraction of open reaction centers were reduced significantly (Table I). In agreement with the standard NPQ and qE measurements (Fig. 6A; Supplemental Fig. S5), NPQt (Tietz et al., 2017) under steady-state growth light conditions was 10-fold higher in P-deficient plants (Table I). No differences in ETR(I), ETR(II), or state transition (Supplemental Table S3) were observed in low light (60 μmol photons m⁻² s⁻¹).

To examine if lumen acidification leads to impaired PQH₂ oxidation at the Cyt *b₆f* complex, we measured the redox state of the PQ pool using OJIP transients (Tóth et al., 2007; Table II). The fraction of reduced PQH₂ was increased significantly for the P-deficient plants relative to the control and P-resupplied plants, indicating a slower oxidation of PQH₂ at the Cyt *b₆f* complex.

Finally, to confirm that an impaired PQH₂ oxidation at the Cyt *b₆f* complex essentially restricts the flow of electrons to PSI (Schlödter and Meyer, 1987), we evaluated P700⁺ reduction kinetics (Fig. 7). P700⁺ reduction was markedly higher in P-deficient plants than in control and P-resupplied plants in growth light conditions (Fig. 7A), but clearly not under high-light (2,200 μmol photons m⁻² s⁻¹) conditions (Fig. 7B). This result confirms that the electron flow to PSI is severely reduced in P-deficient plants under increasing light intensity (Fig. 6, B and C).

DISCUSSION

Latent P deficiency without any observable leaf symptoms was successfully induced with leaf P concentrations as low as 850 μg P g⁻¹ dry weight (Reuter and Robinson, 1997), and chloroplast P_i concentrations were measured between 20 and 40 nmol mg⁻¹ chlorophyll depending on whether plants were light or dark adapted prior to extraction, respectively (Figs. 1 and 4, E and F; Supplemental Fig. S1). This result was fundamentally different from those of previous studies, which induced P-deficient-like conditions by infiltrating leaf segments with Man to strip the entire leaf P_i pool by irreversible phosphorylation (Takizawa et al.,

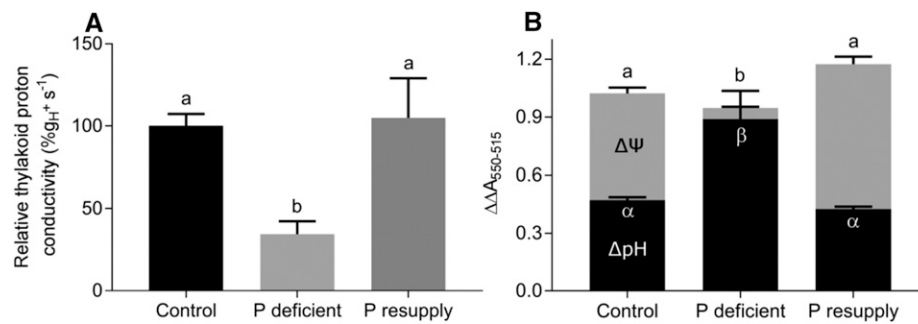


Figure 5. ATP synthase activity and *pmf* partitioning in barley. A, Relative thylakoid proton conductivity, which reflects the activity of ATP synthase. B, Relative *pmf* partitioning in control, P-deficient, and P-resupplied barley plants. Values are means \pm SE ($n = 5$, each with more than four technical replicates), and different letters represent statistically significant changes ($P < 0.05$) using one-way ANOVA and Tukey's multiple comparison test. Greek letters indicate statistical differences in $\Delta p\text{H}$, and Roman letters indicate differences in $\Delta\Psi$.

2008) or used knockout mutants of the Arabidopsis thylakoid membrane P_i transporter PHT4;1 (Karlsson et al., 2015). Unlike previous publications, we quantified the P_i concentration of isolated chloroplasts from P-deficient plants. Such quantification is not trivial, and the values obtained may not exactly reflect the true in vivo values, since some loss of P_i during the extraction process is unavoidable. However, we found it encouraging that P_i concentrations from both light- and dark-adapted chloroplasts showed the same trend relative to the control, P-deficient, and P-resupplied treatments. This provides confidence that the analytical procedure used here is able to reflect the dynamics of chloroplast P_i when plants were exposed to the treatments.

The results presented here indicate that the biological mechanisms reflected by the I-step were achieved by adjusting the P availability in the nutrient solution to obtain physiologically relevant P deficiency responses at the whole-plant level. The establishment of latent P-deficient plants successfully induced a series of fully reversible, but marked, disturbances in the electron flow to PSI and the synthesis of ATP and NADPH. This experimental design allowed us to study how the photosynthetic machinery adapts to long-term P starvation and how rapidly it responds to P resupply and allowed us to construct a biological model summarizing the cascade of events resulting from P deficiency.

P Deficiency Affects Electron Transport beyond PQH₂

P deficiency can be detected based on depletion of the I-step from the fast OJIP region of the chlorophyll *a* fluorescence transient (Fig. 2A). In fact, the response is so sensitive to the leaf tissue P concentration that it can be used to accurately predict bioavailable P in both monocots and dicots (Frydenvang et al., 2015). Several hypotheses have been proposed to explain the biological mechanisms underlying the polyphasic OJIP fluorescence curve. However, despite the general agreement that the O-J phase reflects the light-driven accumulation of Q_A^- (also known as the Q_A model; Strasser and Govindjee, 1992), the

explanation for the J-I-P phase is still speculative and controversial. The predominant theoretical interpretations of the J-I-P phase include fluorescence quenching by the oxidized PQ pool (Lavorel and Etienne, 1977), light-driven accumulation of Q_B^- and Q_B^{2-} (Strasser and Govindjee, 1992), reduction of Q_B and PQ by PSII (Srivastava et al., 1995), direct contributions from PSI fluorescence (Franck et al., 2002), and PSI oxidation (Schansker et al., 2005). It has been suggested that the difference in $\Delta\psi$ could modulate the I-P phase and that it largely influences the fluorescence yield of the J-I-P phase (Vredenberg, 2004; Antal et al., 2011).

The results presented here indicate that the biological mechanisms reflected by the I-step, which is highly responsive to changes in the leaf tissue P concentration, originate from restricted downstream PQH₂ oxidation. Measurements of the PQ pool redox state confirmed an increased fraction of reduced PQH₂ in P-deficient plants (Table II). The I-step disappeared when leaves were infiltrated with DBMIB to inhibit PQH₂ oxidation at the Cyt *b₆f* complex, and similar transients were obtained when bypassing the transient FNR block using MV (Fig. 3A). Comparable observations were reported in a previous study (Schansker et al., 2005) that infiltrated pea (*Pisum sativum*) leaves with DBMIB and MV. The authors stated that a distinct I-P phase required electron transfer beyond the Cyt *b₆f* complex (blocked by DBMIB) and a transient block at the acceptor side of PSI (bypassed by MV). We note that, besides the inhibition of PQH₂ oxidation at the Q_O -binding site of the Cyt *b₆f* complex, DBMIB also might quench chlorophyll excited states of the PSII antenna and act as a PSII electron acceptor, thereby decreasing the reduction of the PQ pool (Belatik et al., 2013). However, with the clear differences between infiltration with DCMU and DBMIB (Fig. 3A) and because no effects were observed on the quantum yield efficiency (data not shown), we are convinced that DBMIB specifically inhibited PQH₂ oxidation under the conditions given in this infiltration study. The two Arabidopsis PSI mutants, *psad1-1* and *psae1-3*, also display severely reduced I-steps, which may reflect the pronounced reductions in the PSI

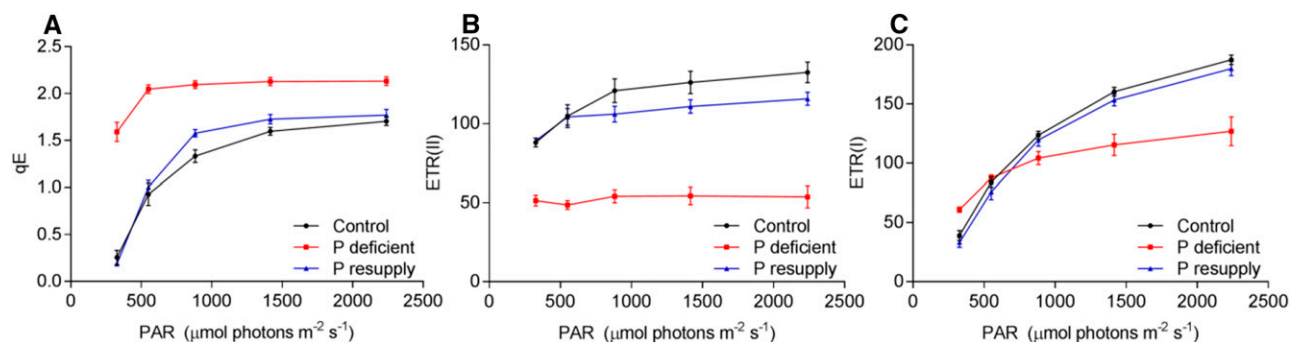


Figure 6. The qE and electron transfer rates at different light intensities in barley. Light-adapted barley plants were exposed to increasing light intensities (red actinic light with a wavelength of 620 nm), starting at growth light. A, The qE component of NPQ. B, ETR(II). C, ETR(I). Values are means \pm SE ($n = 4-5$, each with more than four technical replicates). PAR, Photosynthetically active radiation.

subunits PsaD1 and PsaE1, respectively, that markedly impair photosynthetic electron flow (Ihnatowicz et al., 2004, 2007; Fig. 3B).

These combined results indicate that the inflection at the I-step remains intact when transient equilibrium is attained between PSII-mediated reduction of the PQ pool and its oxidation by the Cyt b_6f complex via electron flow to PSI. The further rise to reach maximum fluorescence at the P-step is achieved when PSI electron acceptors are completely reduced due to a transient block caused by temporarily inactivated FNR, which is induced by the dark adaptation performed before the measurements (Stirbet and Govindjee, 2012). Consequently, reduced inflection at the I-step (and eventually elimination of the I-step) reflects slower electron flow to PSI electron acceptors (Stirbet et al., 2014). This was confirmed by analysis of the P700⁺ reduction rate in similarly dark-adapted plants, which was markedly slower for P-deficient plants than for control plants (Supplemental Fig. S6). Previous work showed that the rate-limiting step in electron transport between the two photosystems is determined by PQH₂ oxidation at the Cyt b_6f complex (Tikhonov, 2014). Electron flow to PSI is reduced when the PQH₂ oxidation rate decreases, which reduces the inflection at the I-step.

Analysis of steady-state P700⁺ reduction rates revealed a higher rate of P700⁺ reduction in P-deficient plants at growth light conditions (Fig. 7A), suggesting that P deficiency up-regulates electron transfer rates in PSI under continuous growth light (Fig. 6C), while PSII

is down-regulated (Table I; Fig. 6B). Since linear electron flow was down-regulated in growth light (Table I) and given that electron transfer rates in PSI reflect the sum of linear (originating from PSII) and cyclic electron flow, the results suggest that cyclic electron flow is up-regulated at steady-state growth light conditions in P-deficient plants. Electron transfer rates of PSI remained similar to those of the control in low light (Supplemental Fig. S7; Supplemental Table S3) but became highly down-regulated in high light (Figs. 6C and 7B), when luminal pH is expected to significantly acidify.

P Deficiency Alters ATP and NADPH Synthesis

In contrast to the highly dynamic P_i levels observed at the leaf tissue level, we observed strong homeostatic regulation of the chloroplast P_i pool (Fig. 4, D–F). P deficiency resulted in a marked 4-fold decrease in leaf tissue P_i , whereas P_i in isolated chloroplasts was reduced by only approximately 20% to 40% depending on whether plants were dark or light adapted prior to extraction, respectively. These results suggest that vacuoles contain a storage pool of nonmetabolic P_i under adequate P conditions, whereas most of the P_i is sequestered in the metabolic pool in chloroplasts under P-deficient conditions (Lauer et al., 1989). Three P_i transporter families are localized in the chloroplast to supply P_i in the stroma, where PHT4;1 is the only transporter localized in the thylakoid membrane.

Table I. Photosynthetic parameters measured under steady-state growth light conditions

The plants were light adapted in growth light ($300 \mu\text{mol photons m}^{-2} \text{s}^{-1}$) for a minimum of 8 h and measured afterward using the Leaf Photosynthesis MultispeQ V1.0 protocol with the MultispeQ from PhotosynQ. The results are means \pm SE ($n = 4-5$, each with more than four technical replicates), and different letters represent statistically significant changes ($P < 0.05$) using one-way ANOVA and Tukey's multiple comparison test. ϕ (II), PSII quantum yield; ϕ (NPQ), NPQ quantum yield; LEF, linear electron flow; qP, fraction of open reaction centers; NPQt, NPQ estimation without dark adaptation; ϕ (NO), fraction of energy absorbed by PSII that is lost to unregulated processes.

Treatment	ϕ (II)	ϕ (NO)	ϕ (NPQ)	LEF	qP	NPQt
Control	0.53 \pm 0.01 a	0.31 \pm 0.01 a	0.16 \pm 0.01 a	79.48 \pm 3.66 a	0.69 \pm 0.02 a	0.54 \pm 0.02 a
P deficient	0.30 \pm 0.02 b	0.13 \pm 0.01 b	0.57 \pm 0.03 b	45.22 \pm 4.29 b	0.60 \pm 0.02 b	5.11 \pm 0.69 b
P resupply	0.47 \pm 0.02 a	0.33 \pm 0.02 a	0.19 \pm 0.01 a	77.39 \pm 3.09 a	0.63 \pm 0.03 a,b	0.60 \pm 0.03 a

Table II. The plastoquinone (PQ) pool redox state in barley leaves

Estimation of the fraction of reduced PQ was determined using OJIP transients. The results are means \pm SE ($n = 4$, each with four technical replicates), and different letters represent statistically significant changes ($P < 0.05$) using one-way ANOVA and Tukey's multiple comparison test.

Treatment	Fraction of PQH ₂
Control	0.27 \pm 0.01 a
P deficient	0.36 \pm 0.02 b
P resupply	0.28 \pm 0.01 a

Furthermore, a limitation in ATP synthase and reduced growth has only been demonstrated for PHT4;1 mutants (Karlsson et al., 2015). PHT4;1 mediates the availability of P_i for ATP synthesis in the chloroplast stroma (Karlsson et al., 2015), and it is likely that the P_i concentration in chloroplasts is regulated by effective phosphate homeostasis to maintain ATP synthesis and drive the Calvin cycle (Mimura et al., 1990).

P_i in the chloroplast stroma functions as a substrate for ATP synthesis. P deficiency significantly reduces P_i levels and significantly reduces ATP production in isolated thylakoids (Fig. 4C). This was further supported by significant reductions in the rate constant of ATP synthase (Fig. 5A) as a response to the low P_i concentration in chloroplasts. These observations confirmed the modulated response of ATP synthase activity to metabolic or physiological conditions, allowing the regulation of light and assimilatory reactions (Strand and Kramer, 2014). The NADP⁺ levels, acting as a substrate for the production of NADPH, also were reduced significantly by P deficiency (Fig. 4A), indicating that a larger fraction of NADP⁺ remains in the reduced form (NADPH), because it cannot be utilized in the Calvin cycle due to ATP limitation and because of a higher PSI activity (Fig. 7A). This hypothesis was supported by the total NADPH concentration, which was significantly higher for the P-deficient treatment than for the control and P-resupply treatments (Fig. 4B).

The K_m for ATP synthase is expected to range between 0.6 and 1 mM P_i; therefore, lowering the P_i concentration in the chloroplast stroma to levels near K_m is expected to slow ATP synthesis and increase Δ pH (Takizawa et al., 2008). Assuming a chloroplast volume of 25 μ L mg⁻¹ chlorophyll

(Sharkey and Vanderveer, 1989), the P_i concentrations for chloroplasts extracted after light adaptation correspond to 1.1 and 0.7 mM P_i for the control and P-deficient treatments, respectively, which is in the same range as previous reports using colorimetric assays (Robinson and Giersch, 1987; Sharkey and Vanderveer, 1989; Fig. 4E) and clearly within the range that would affect ATP synthesis. Thus, our results show that ATP synthase activity is very sensitive to changes in the P_i concentration in chloroplasts and that even minor reductions in stromal P_i concentration have a major influence on ATP synthase activity, which strongly reduces proton efflux from the lumen.

P Deficiency Induces Lumen Acidification and Prevents PQH₂ Oxidation

The reduced rate constant of ATP synthase under P-deficient conditions limits the export of protons to the chloroplast stroma, thereby markedly acidifying the thylakoid lumen (Fig. 5B). As a consequence, the PQH₂ oxidation at the Cyt *b₆f* complex was impaired for the P-deficient plants (Table II), which further decreased the linear electron flow toward PSI (Table I). This lumen acidification also was reflected by a much faster quenching of the chlorophyll *a* fluorescence intensity after reaching its maximum (Fig. 2A), an increase in qE (Fig. 6A), and a higher NPQ (Table I; Supplemental Fig. S5). These observations were further supported by the PSMT decay phase of the extended chlorophyll *a* fluorescence transient (Supplemental Fig. S4). In addition to increased fluorescence quenching, chlorophyll *a* fluorescence transients of P-deficient plants also lacked the S-step. A previous study of isolated chloroplasts of pea leaves identified a linear relationship between P-S quenching and lumen acidification (Briantais et al., 1979), and a more recent study concludes that formation of the S-step is associated with increased Δ pH (Goltsev et al., 2016). These combined data strongly support our hypothesis that P deficiency at physiologically relevant concentrations causes lumen acidification in both light- and dark-adapted plants.

A reduction in lumen pH provides the key signal to regulate light capturing via NPQ components (Ruban, 2016), and this study confirmed the relationship between NPQ and lumen acidification induced by P deficiency

Figure 7. P700⁺ reduction kinetics in barley. A, P700⁺ reduction in growth light conditions. B, P700⁺ reduction in high-light conditions. Plants were light adapted for more than 2 h prior to measurements, then preilluminated with red actinic light (620 nm) for 3 min, followed by a 10-ms dark pulse. The plotted transients are averaged ($n = 5$, each with more than four technical replicates). A.U., Arbitrary units.

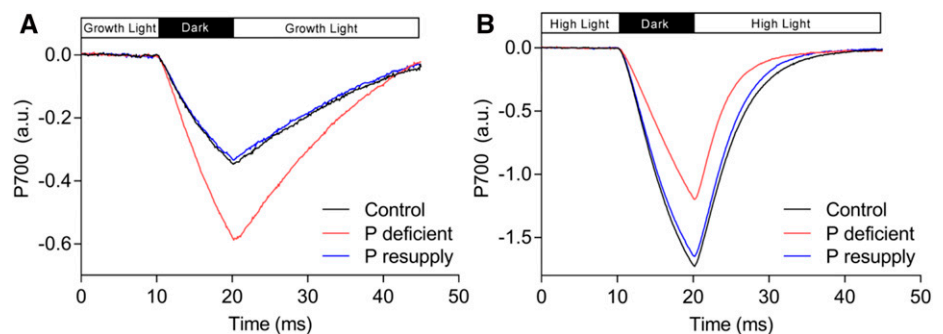


(Table I; Supplemental Fig. S5). These adaptive mechanisms enhance the dissipation of excess energy captured by the light-harvesting antenna to protect the photosynthetic apparatus (Stirbet and Govindjee, 2011). The oxygen-evolving complex of PSII is particularly affected by lumen acidification (Schlodder and Meyer, 1987). The PSII quantum yield determined from chlorophyll *a* fluorescence transients of dark-adapted leaves was not affected by P deficiency (Fig. 2A). However, to determine the influence of ΔpH on PSII quantum yield and ETR(II) in light, we also performed measurements on light-adapted leaves (Table I; Fig. 6B). Here, it is clearly evident that the PSII quantum yield is reduced markedly by P deficiency but recovers after a subsequent dark-adaptation period, which highlights the highly reversible response to P deficiency in plants.

CONCLUSION

The reversible nature of the disruptions in photosynthesis caused by P deficiency allows us to build a comprehensive biological model summarizing the effects of P deficiency on photosynthesis (Fig. 8). P is the substrate for ATP synthesis in the chloroplast stroma. When the P_i substrate is lacking due to low P availability (Figs. 1 and 4, D–F), ATP synthase activity decreases (Fig. 5A), which reduces ATP production in the stroma and CO_2 fixation (Figs. 4C and 8B, steps 1 and 2). Reduced ATP synthase activity reduces the flow of protons from the thylakoid lumen to the chloroplast stroma, which causes lumen acidification (Figs. 5B and 8B, step 3). Lumen acidification triggers energy dissipation via NPQ (Table I; Supplemental Fig. S5), where the major and most rapid component (qE) is responsible

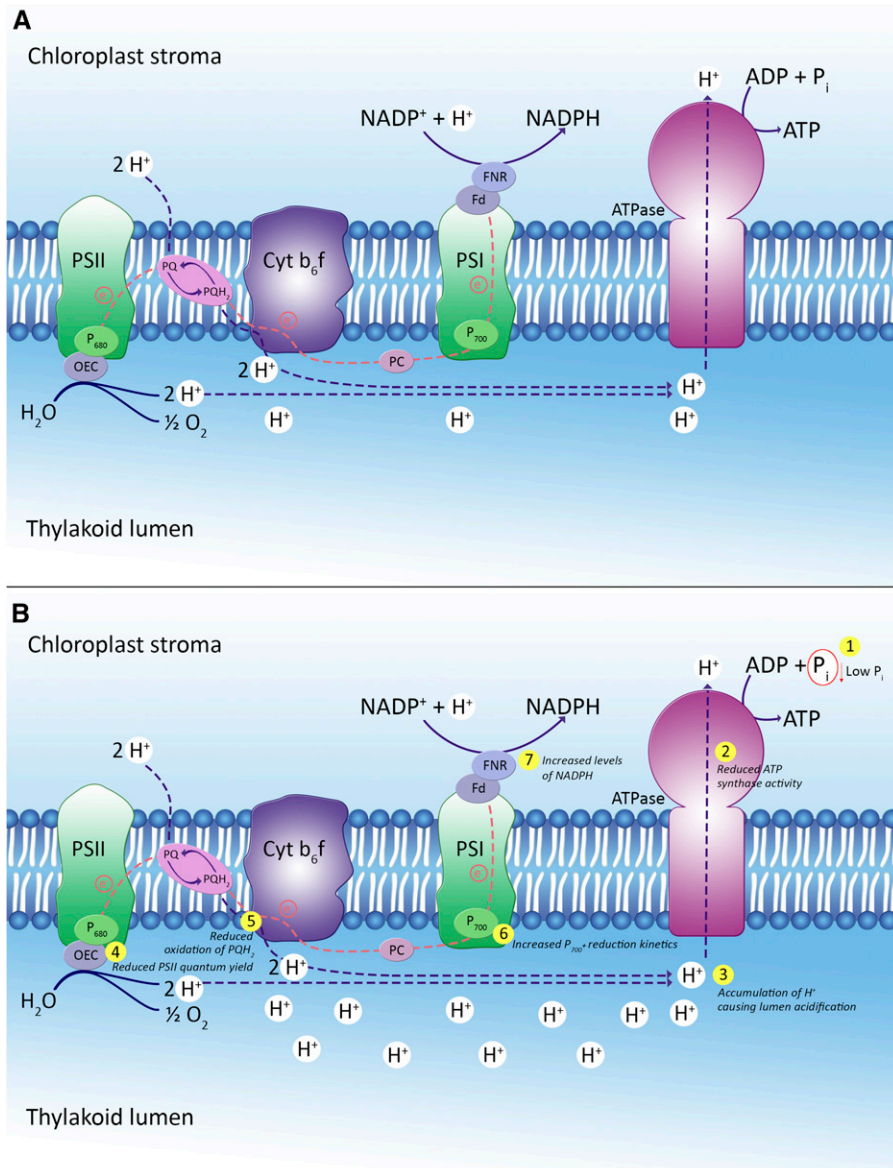


Figure 8. Photosynthetic regulation in response to P deficiency at growth light conditions. A, Photosynthetic electron flow under P-sufficient conditions. B, Feedback mechanisms responsible for reduced electron flow from PSII to PSI under P-deficient conditions. See text for further explanation of the cascade of events highlighted in steps 1 to 7. OEC, Oxygen-evolving complex.

for the efficient quenching of fluorescence (Figs. 2A and 6A; Supplemental Fig. S4) and reduces the PSII quantum yield (Table I; Figs. 6B and 8B, step 4; Supplemental Fig. S5). Acidification of the thylakoid lumen was found to decelerate PQH₂ oxidation at the Cyt *b₆f* complex (Table II; Fig. 8B, step 5) and is likely to represent a bottleneck in overall electron transport from PSII to PSI (Tikhonov, 2013; Strand and Kramer, 2014). This causes protonation of the donor side of Cyt *b₆f* and reduces the probability of PQH₂ oxidation, ultimately reducing the linear electron flow to PSI (Tikhonov, 2014; Table I; Fig. 6B). Finally, P700⁺ reduction is either decreased under high light (2,200 μmol photons m⁻² s⁻¹; Fig. 7B) or increased in steady-state growth light (300 μmol photons m⁻² s⁻¹; Figs. 7A and 8B, step 6), which ultimately increases the NADPH levels (Figs. 4, A and B, and 8B, step 7). Thus, depletion of the I-step phase from the OJIP region of the chlorophyll *a* fluorescence transient under P deficiency is likely to reflect a restricted PQH₂ oxidation due to the proton backlog caused by lumen acidification.

MATERIALS AND METHODS

Plant Cultivation and Sampling

Barley (*Hordeum vulgare* 'Quench') plants were cultivated in hydroponics as described previously (Frydenvang et al., 2015). Barley seeds were pregerminated in vermiculite in a greenhouse with minimum day/night temperatures of 18°C/15°C and a day/night cycle of 16 h/8 h (minimum 300 μmol photons m⁻² s⁻¹ light intensity). After 7 d, four seedlings were placed in a lid, transferred to a 4-L hydroponic container, and kept at the same climatic conditions throughout the whole experiment. Control plants were supplied with a nutrient solution containing 200 μM KH₂PO₄, 200 μM K₂SO₄, 300 μM MgSO₄·7H₂O, 100 μM NaCl, 300 μM Mg(NO₃)₂·6H₂O, 900 μM Ca(NO₃)₂·4H₂O, 600 μM KNO₃, 50 μM Fe(III)-EDTA-Na, 2 μM H₃BO₃, 0.8 μM Na₂MoO₄·2H₂O, 0.7 μM ZnCl₂, 1 μM MnCl₂·4H₂O, and 0.8 μM CuSO₄·5H₂O. The P-deficient plants were supplied with the same nutrient solution as stated above, but with only 9 μM KH₂PO₄ throughout the growth period. All nutrients were prepared in Milli-Q water (Milli-Q Element; Millipore). The nutrient solutions were changed weekly and aerated using steel medical syringes, and the pH of the solution was maintained at 6 ± 0.3 using ultrapure HCl.

Four containers holding a total of 16 plants received the full nutrient solution throughout the experiment (control), and eight containers holding a total of 32 plants received the P-deficient solution. After either 21 or 25 DAP, four P-deficient containers holding a total of 16 plants were resupplied with P corresponding to the control level (200 μM KH₂PO₄) and the remaining four containers continued to receive the P-deficient solution. All plants were harvested at 28 DAP, either 3 or 7 d after P resupply. Each treatment included four hydroponic pots containing four barley plants each (i.e. 16 plants for each treatment). All plants were kept in a dark room the night before harvest, exposed to 1 h of light, and then harvested. One YFEL from each plant was dried and used for elemental analysis, one YFEL was used directly to determine the NADP⁺ concentration, and one YFEL was harvested after 8 h of growth conditions for starch determination. The remaining YFELs were harvested 1 h after the onset of light, quickly frozen in liquid nitrogen, and subsequently used to isolate thylakoid membranes. An identical treatment of plants was used entirely for isolating chloroplasts. Chlorophyll *a* fluorescence was measured before P resupply at 21 DAP and before harvest at 28 DAP, when pulse amplitude modulation measurements also were performed. All analyses were performed with a minimum of four biological replicates.

Arabidopsis Mutants

Seeds of Arabidopsis (*Arabidopsis thaliana*) mutants *psad1-1* (Ihnatowicz et al., 2004) and *psae1-3* (Ihnatowicz et al., 2007) and the wild type were sown directly in pots (5.5 cm diameter) containing prewetted Pindstrup Substrate No.

2 (Pindstrup Mosebrug) in a climate chamber with minimum day/night temperatures of 23°C/18°C and a day/night cycle of 8 h/16 h (150 μmol photons m⁻² s⁻¹ light intensity). The pots were sealed during the first 7 d to increase humidity and were watered when needed. Chlorophyll *a* fluorescence transients were measured after 6 weeks of growth.

Chlorophyll *a* Fluorescence, P700, and ECS

Chlorophyll *a* fluorescence transients (OJIP transients) were obtained from YFELs using a Handy PEA chlorophyll fluorometer (Hansatech Instruments). The YFEL midsection was dark adapted for at least 25 min before measurements, which were obtained using Hansatech leaf clips, and a short nonactinic light flash was applied to the leaf to adjust the detector gain. Each leaf sample was illuminated with continuous saturating actinic light (3,000 μmol photons m⁻² s⁻¹) from three LEDs, and the fluorescence transients were recorded using a PIN photodiode. The fluorescence signal was measured for either 2 or 10 s. To measure the slow PSMT phase, the incident light was 1,000 μmol photons m⁻² s⁻¹ and the fluorescence transient was measured for 30 s. All transients were double normalized between F₀ and F_m to give the relative variable fluorescence at time *t* as follows: $V(t) = [\text{Fluorescence}(t) - F_0] / (F_m - F_0)$.

ECS, pulse amplitude-modulated chlorophyll *a* fluorescence, and P700 measurements were carried out using a Walz Dual-PAM 100 equipped with P515/535, DUAL-DB, and DUAL-E emitter-detector modules. The rate constant of ATP synthase (g_{H^+} s⁻¹) and *pmf* partitioning ($\Delta\Psi$ and ΔpH) was determined on plants that were dark adapted for a minimum of 1 h followed by 1 min of illumination with actinic red light of 339 μmol photons m⁻² s⁻¹. The g_{H^+} parameter was calculated as 1/decay time constant, which was derived from single exponential fittings of the ECS decay signal during an 80-ms dark pulse (Cruz et al., 2005) after 1 min of illumination. *pmf* (ECS_T) partitioning to $\Delta\Psi$ (ECS_{SS}) and ΔpH (ECS_{INV}) was calculated from a 60-s dark interval relaxation kinetics of the ECS signal (Cruz et al., 2001). ECS_T was calculated as the difference between the ECS signal in light and the minimum value of the ECS signal after the light was turned off. Calculation of ECS_{SS} and ECS_{INV} was performed using either the steady-state time point of the ECS signal in darkness or the time point before the ECS signal decays again due to changes in pigment composition. For calculation of the results presented in Figure 5B, see Supplemental Figure S8. Before each ECS measurement, a saturating 50-μs flash of 200,000 μmol photons m⁻² s⁻¹ was applied to determine the ECS_{50μs}; subsequently, the ECS_{50μs} amplitude was used to normalize the dark interval relaxation kinetics ECS signal before calculation of *pmf* size and partitioning values. Therefore, $\Delta\Delta_{A550-515}$ represents the normalized ECS signal to ECS_{50μs}. NPQ and PSII quantum yield were measured using plants that had been dark adapted for 30 min, illuminated with high light (1,700 μmol photons m⁻² s⁻¹) for 5 min, and then held for 4 min of dark relaxation. qE was calculated as the difference between NPQ after 3 min of illumination and NPQ after 5 min of subsequent dark adaptation. P700 oxidation-reduction kinetics were recorded on plants that had been dark adapted for a minimum of 1 h, illuminated with far-red light for 30 s, and then saturated with a pulse of actinic red light (20,000 μmol photons m⁻² s⁻¹) for 1 s. ETR(I) was calculated as $\nu P700$ s⁻¹ according to Strand et al. (2017) by fitting a linear function on the initial decay of the P700 signal upon applying a dark pulse. $\nu P700$ s⁻¹ was determined on leaves preilluminated with actinic red light (620 nm; Figs. 6C and 7; Supplemental Fig. S7) or actinic red light and far-red light (730 nm; Supplemental Fig. S7). State transition was carried out according to Lunde et al. (2000) at 60 μmol photons m⁻² s⁻¹; the qS parameter was calculated according to Damkjaer et al. (2009).

Leaf Infiltration with P and Chemical Electron Inhibitors

The YFELs of 28-d-old P-deficient barley plants were cut into 5-cm sections and immersed in 1 M KH₂PO₄ containing 0.2 mL L⁻¹ Tween 20 for 1 h. Then, the leaf sections were removed from the immersion solution and gently wiped to remove excess moisture, placed in a zip bag, and dark adapted for 25 min. As a control, leaves from the same plant treatment were immersed in Milli-Q water containing 0.2 mL L⁻¹ Tween 20.

YFELs of 28-d-old control barley plants were infiltrated with 200 μM DCMU, 900 μM DBMIB, or 200 μM MV as described previously (Schansker et al., 2005). DCMU and DBMIB were solubilized in 1% (v/v) ethanol. The leaves were cut into 3-cm sections and immersed in the respective solutions for 3 h. Subsequently, the sections were placed in zip bags and dark adapted for 25 min before recording chlorophyll *a* fluorescence. Control leaves were treated in the same way without adding the chemical electron inhibitors.

NADP⁺ and NADPH Assays

The NADP⁺ concentration was determined as described previously (Queval and Noctor, 2007), and every step was performed at 4°C. A total of 100 mg of fresh YFELs from each replicated treatment was harvested at 28 DAP and rapidly frozen in liquid nitrogen. Then, 1 mL of ice-cold 0.2 N HCl was added to a mortar with quartz sand, and the plant material was thoroughly ground and centrifuged at 16,000g for 10 min at 4°C. A 0.2-mL aliquot of the supernatant was incubated in boiling water for 1 min and then rapidly cooled. The aliquot was neutralized by adding 20 μ L of 0.2 M NaH₂PO₄ (pH 5.6), followed by stepwise addition of 0.2 M NaOH to reach a final pH of between 5 and 6. Then, 30 μ L of the neutralized supernatant was introduced to a 96-well plate, in which each well contained 0.1 mL of 0.1 M HEPES (pH 7.5) and 2 mM EDTA, 20 μ L of 1.2 mM dichlorophenolindophenol, 10 μ L of 20 mM phenazine methosulfate, 10 μ L of 10 mM Glc-6-P, and 30 μ L of Milli-Q water. NADP⁺ concentrations ranging from 0 to 100 pmol were used as standards. The reaction was started by adding 10 μ L of Glc-6-P dehydrogenase (200 units mL⁻¹), the plate was swirled rapidly and placed on an EON microplate spectrophotometer (BioTek Instruments), and the A₆₀₀ was measured every 23 s for 5 min. The rates during the first 2 min were used to determine the final NADP⁺ concentration according to the relevant standards and blank correction.

The NADPH concentration was determined using the NADP/NADPH Quantification Kit (Sigma-Aldrich; catalog no. MAK038) following the protocol from the manufacturer. An EON microplate spectrophotometer (BioTek Instruments) was used to measure the A₄₅₀ after 2 h of incubation.

Isolation of Thylakoid Membranes

All extractions were performed at 4°C under dim-green light conditions to maintain thylakoid integrity. Frozen YFELs were homogenized in 200 mL of buffer solution containing 0.4 M Suc, 10 mM NaCl, 5 mM MgCl₂, 20 mM Tricine (pH 7.9), 10 mM L-ascorbate, and 10 mM NaF using a laboratory blender (Waring Laboratory; LB20E). The homogenate was filtered through a double layer of Miracloth (pore size, 22–25 μ m). The extracts were centrifuged for 10 min at 6,000g, the supernatant was discarded, and the pellet was resuspended in 5 mM Tricine (pH 7.9) and 10 mM NaF. The washed thylakoids were pelleted by centrifugation for 10 min at 11,200g and resuspended in a storage solution containing 0.4 M Suc, 10 mM NaCl, 5 mM MgCl₂, 20 mM Tricine (pH 7.9), 10 mM NaF, and 20% (v/v) glycerol. The samples were immediately frozen in liquid nitrogen and stored at -80°C.

Determination of Protein and Chlorophyll Contents in Thylakoid Membranes

The protein content in the isolated thylakoid membranes was determined using the Pierce BCA Protein Assay Kit (Thermo Fisher Scientific), and an EON microplate spectrophotometer (BioTek Instruments) was used to measure the A₅₆₂. To determine the chlorophyll concentration, 5 μ L of the isolated thylakoid membrane was diluted in 995 μ L of ice-cold 80% (v/v) acetone, incubated on ice for 15 min, and centrifuged for 2 min at 10,000g in a tabletop microcentrifuge (Eppendorf Minispin Plus) to pellet proteins. The absorbance at 647 and 664 nm was measured using a Genesys 10S UV-VIS spectrophotometer (Thermo Fisher Scientific), and the total chlorophyll concentration (μ g mL⁻¹) was calculated as $(17.76 \times A_{647}) + (7.34 \times A_{664})$ multiplied by the dilution factor (Porra et al., 1989).

Chloroplast Isolation

Plants were either dark adapted for 10 h or light adapted at growth conditions for 4 h prior to isolation. All extractions were performed at 4°C under dim-green light conditions. All YFELs from each replicate were cut into 3- to 4-cm sections, placed in a blender containing 200 mL of ice-cold HS buffer (50 mM HEPES and 330 mM sorbitol, adjusted to pH 8 with KOH pellets), and rapidly blended with three quick bursts. The homogenate was filtered through a double layer of Miracloth (pore size, 22–25 μ m) and centrifuged at 3,300g for 2 min in a swing rotor (Heraeus Megafuge 16R; Thermo Fisher Scientific) with slow acceleration and without brakes for deceleration. The supernatant was carefully discarded, and the tubes were rolled on ice to loosen the pellets. Then, 1 mL of HS buffer was added, and the suspension was layered onto a precooled Percoll pad containing 2 mL of 5 \times HS buffer, 3.5 mL of Percoll, and 4.5 mL of Milli-Q water and centrifuged at 1,400g for 8 min in a swing rotor. The green middle layer (containing thylakoids and broken chloroplasts) and the Percoll were removed carefully, leaving the pelleted intact chloroplasts. The pellet was suspended in

10 mL of HS buffer and centrifuged at 3,000g for 2 min in a swing rotor. The supernatant was discarded, and the pellet was suspended in 700 μ L of HS buffer and stored at -80°C until use.

Determination of Chlorophyll Content in Isolated Chloroplasts

The chlorophyll concentration in the isolated chloroplasts was determined by adding 10 μ L of chloroplasts to 990 μ L of ice-cold 80% (v/v) acetone, mixing the solution, and centrifuging for 30 s at 10,000g in a tabletop microcentrifuge (Eppendorf Minispin Plus) to pellet the proteins. The A₆₅₂ was measured using a Genesys 10S UV-VIS spectrophotometer (Thermo Fisher Scientific). The chlorophyll concentration (μ g mL⁻¹) was determined using the following equation: A₆₅₂ \times 5.6 (Robinson and Mant, 2002).

Determination of the PQ Pool Redox State

A noninvasive assay of the PQ pool redox state was performed following the protocol from Tóth et al. (2007). To obtain fully reduced PQ pools, OJIP transients were measured at saturating actinic light (3,000 μ mol photons m⁻² s⁻¹) as described above. To obtain fully oxidized PQ pools, leaves were preilluminated with far-red light (200 μ mol photons m⁻² s⁻¹) for 10 s, and a second OJIP transient was measured immediately after. From the first OJIP transient, the F_J (fluorescence intensity after 3-ms J-step) and F_m values were extracted, whereas the F_{J-ox} (representing the fully oxidized PQ pool at 3 ms) was extracted from the far-red light treatment. The fraction of reduced PQ was calculated using the following equation: $(F_J - F_{J-ox}) / (F_m - F_{J-ox})$, where 0 and 1 represent a fully oxidized and a fully reduced PQ pool, respectively.

ATP Assay

ATP concentrations were determined in thylakoid membranes as described previously (Grennan and Ort, 2011). A thylakoid membrane aliquot containing 20 μ g of chlorophyll was resuspended in 1 mL of buffer containing 500 mM Tricine-NaOH (pH 8), 500 mM NaCl, 5 mM MgCl₂, 0.05 mM phenazine methosulfate, 2 mM K₂HPO₄ (pH 7), 1 mM ADP (ATP free), and 0.1 mM diadenosine pentaphosphate. The reaction was carried out with incident light at 300 μ mol m⁻² s⁻¹ for 2 min at room temperature. Then, the light was switched off and the reaction was stopped by adding trichloroacetic acid to a final volume of 0.5% (w/v). The samples were centrifuged at 11,200g for 5 min at room temperature. The supernatant was assayed for ATP concentration by measuring chemiluminescence using a ChemiDoc Touch Imaging System (Bio-Rad). A 100- μ L aliquot of the supernatant was added to a 96-well plate, and 100 μ L of a second buffer containing 25 mM Tris acetate (pH 7.75), 2 mM EDTA, 50 mM DTT, 0.02 mM D-luciferin, 1.5 mg mL⁻¹ BSA, 20 mM magnesium acetate, and 0.3 μ g mL⁻¹ luciferase was quickly added to each well. The chemiluminescence was measured during a 20-min period, and the signal was integrated using Image Lab software (version 5.2.1; Bio-Rad). The same reaction mix was used to determine ATP standards dissolved in 25 mM Tris acetate (pH 7.75).

P_i Quantification

P_i was quantified by HPLC as described previously (Hawkesford et al., 2013). A total of 100 mg of dried YFEL material was added to 1.5 mL of Milli-Q water and heated in a heating block at 80°C for 4 h with frequent shaking. To quantify P_i in isolated chloroplasts, a chloroplast preparation containing 20 μ g of chlorophyll in 200 μ L of HS buffer was heated directly in a heating block at 80°C for 4 h. The samples were allowed to cool and then centrifuged at room temperature at 13,000g for 20 min. The supernatant was transferred to a 2-mL Eppendorf tube and placed at -20°C overnight. After thawing, the sample was centrifuged as before, and the supernatant was filtered using a 0.22- μ m centrifuge tube filter (Spin-X; Costar) at 2,000g for 20 min. This sample was injected onto the HPLC column.

The samples were analyzed on the HPLC Dionex ICS-2100 Anion (Thermo Fisher Scientific) column using the Dionex AS-AP autosampler, Dionex EGC III KOH eluent generator, AERS 2-mm suppressor, and DS6 heated conductivity cell. Anions were separated on a Dionex IonPac AS11-HC RFIC analytical column (2 \times 250 mm) with a Dionex IonPac AG11-HC RFIC guard (2 \times 50 mm) column in front, with 0.38 mL min⁻¹ isocratic flow of 25 mM hydroxide for 15 min. The suppressor was set to 24 mA, and 25 μ L was injected per sample.

The standard curve was generated with five concentrations of Dionex Combined Seven Anion Standard I (Thermo Fisher Scientific) from 0.15 to 2 mg L⁻¹ in HS buffer. Chromeleon 7.2 SR4 software was used for instrument control and data processing.

Starch Quantification

The starch concentration was determined as described previously (Smith and Zeeman, 2006). Frozen YFELs were ground to a fine powder, 5 mL of 80% (v/v) ethanol was added, and the sample was placed in a boiling water bath for 3 min. The samples were centrifuged at 3,000g for 10 min at room temperature, and the supernatant was discarded. The ethanol extraction was repeated another two times, and the ethanol was allowed to evaporate from the final pellet. The pellet was transferred to a mortar, homogenized to a smooth consistency, and transferred to a Falcon tube along with 5 mL of Milli-Q water that was used to wash the mortar. Then, 0.5 mL of the homogenate was added to each of four Eppendorf tubes and heated at 100°C for 10 min. The samples were allowed to reach room temperature, and then 0.5 mL of 200 mM sodium acetate (pH 5.5) was added. In another tube, 6 units of α -amylglucosidase and 0.5 units of α -amylase were dissolved in buffer containing 0.05 mM Tris base, 0.15 mM NaCl, and 0.1% Tween 20 (pH adjusted to 7.6 using HCl); 1.2 mL of this enzyme preparation was added to two of the prepared Eppendorf tubes. The other two Eppendorf tubes were used as controls, which received 1.2 mL of buffer without the enzymes. The samples were incubated at 37°C for 4 h and centrifuged at 10,000g for 5 min at room temperature. The supernatant was assayed for Glc using a Glucose (HK) Assay Kit (Sigma-Aldrich). The assay reagents were mixed, and the reactions were incubated for 15 min at room temperature before measuring the A_{340} using a Genesys 10S UV-VIS spectrophotometer (Thermo Fisher Scientific).

Immunoblot Analysis

Thylakoid samples (containing 5 μ g of protein) were subjected to SDS-PAGE using 12% Criterion TGX Stain-Free precast gels (Bio-Rad) and Tris/Gly/SDS running buffer (Bio-Rad) at a constant voltage of 250 V for 30 min. The proteins were then transferred to a 0.2-mm PVDF membrane using the Trans-Blot Turbo Transfer System (Bio-Rad) according to the manufacturer's instructions. Subsequently, the membrane was blocked for 1 h in 5% (w/v) skimmed milk in PBS-T buffer and incubated overnight in the primary antibody. All primary antibodies (FNR, FDX1, PsaA, PsaF, Cyt f, D1, and CP43) were obtained from Agrisera. The blot was washed three times for 5 min in PBS-T buffer and then incubated with a swine anti-rabbit horseradish peroxidase-conjugated secondary antibody (1:5,000 dilution in PBS-T; Pierce) for 1 h. The blot was washed three times for 5 min in PBS-T buffer, and the secondary antibody was detected using Clarity Western ECL chemiluminescent substrate (Bio-Rad) and the ChemiDoc Touch Imaging System (Bio-Rad). The protein bands were detected and quantified using Image Lab software (version 5.2.1; Bio-Rad).

Transmission Electron Microscopy

The YFELs from three replicated treatments in both dark and light conditions were used for transmission electron microscopy analysis. Leaf discs (1–2 mm²) were fixed in Karnovsky's solution (4% [v/v] paraformaldehyde, 5% [v/v] glutaraldehyde, and 0.1 M sodium cacodylate buffer, pH 7.3) for 4 h and washed three times with buffer (0.1 M sodium cacodylate buffer, pH 7.3). Samples were post-fixed with 1% [v/v] OsO₄ overnight at 4°C. The samples were washed twice with buffer and water and subsequently dehydrated with a graded acetone series. The leaf samples were embedded in Spurr's low-viscosity resin. Ultrathin sections of 60 nm were cut with a diamond knife using a Leica EM-UC7 ultramicrotome and mounted on Pioloform-coated copper grids. The samples were contrasted with 1% [v/v] uranyl acetate and lead citrate and viewed using a Philips CM100 transmission electron microscope at an acceleration voltage of 80 kV. The images were captured using a high-resolution Morada digital camera system.

Elemental Analyses

Leaf element concentrations were determined using inductively coupled plasma-optical emission spectroscopy (5100; Agilent Technologies) equipped with a Meinhard nebulizer and a cyclonic spray chamber. The YFELs were oven dried at

50°C until complete dryness and digested with ultrapure acids (70% [v/v] HNO₃ and 30% [v/v] H₂O₂) at 240°C and 200 bars for 15 min in a pressurized microwave oven (Ultrawave; Milestone). Certified reference material (NIST1515, apple [*Malus* spp.] leaf; National Institute of Standards and Technology) was included to evaluate data quality. Data were processed using Agilent ICP Expert software.

Data Analyses

Statistical analysis was performed using GraphPad Prism 6.0 for Windows. Each mean was compared using one-way ANOVA with Tukey's multiple comparison test. Samples were considered as significantly different at $P < 0.05$.

Supplemental Data

The following supplemental materials are available.

Supplemental Figure S1. Appearance of barley plants cultivated in hydroponics.

Supplemental Figure S2. Transmission electron microscopy of barley leaves.

Supplemental Figure S3. Immunoblot analysis of photosynthetic proteins in barley leaves.

Supplemental Figure S4. OJIPSMT transients of the youngest, fully expanded leaves of barley plants.

Supplemental Figure S5. NPQ and PSII quantum yield in barley leaves.

Supplemental Figure S6. P700⁺ reduction kinetics in barley plants.

Supplemental Figure S7. P700⁺ reduction kinetics in barley under low light.

Supplemental Figure S8. Examples of analysis of raw data leading to the data presented in Figure 5B.

Supplemental Table S1. Element concentrations in the YFELs.

Supplemental Table S2. Quantification of immunoblots of thylakoid protein extracts.

Supplemental Table S3. State transition parameters and electron transfer rates in low light.

ACKNOWLEDGMENTS

We thank Lena Byrgesen and Thomas H. Hansen for assistance with the inductively coupled plasma-optical emission spectroscopy analyses and Birgit Andersen for assistance with the HPLC measurements. Transmission electron microscopy was performed at the Center of Advanced Bioimaging, University of Copenhagen.

Received November 11, 2017; accepted February 25, 2018; published March 14, 2018.

LITERATURE CITED

- Antal TK, Osipov V, Matorin DN, Rubin AB (2011) Membrane potential is involved in regulation of photosynthetic reactions in the marine diatom *Thalassiosira weissflogii*. *J Photochem Photobiol B* **102**: 169–173
- Baker A, Ceasar SA, Palmer AJ, Paterson JB, Qi W, Muench SP, Baldwin SA (2015) Replace, reuse, recycle: improving the sustainable use of phosphorus by plants. *J Exp Bot* **66**: 3523–3540
- Belatik A, Joly D, Hotchandani S, Carpentier R (2013) Re-evaluation of the side effects of cytochrome b6f inhibitor dibromothymoquinone on photosystem II excitation and electron transfer. *Photosynth Res* **117**: 489–496
- Briantais JM, Veronotte C, Picaud M, Krause GH (1979) A quantitative study of the slow decline of chlorophyll a fluorescence in isolated chloroplasts. *Biochim Biophys Acta* **548**: 128–138
- Cordell D, Drangert JO, White S (2009) The story of phosphorus: global food security and food for thought. *Glob Environ Change* **19**: 292–305
- Cordell D, White S (2015) Tracking phosphorus security: indicators of phosphorus vulnerability in the global food system. *Food Secur* **7**: 337–350
- Cruz JA, Avenson TJ, Kanazawa A, Takizawa K, Edwards GE, Kramer DM (2005) Plasticity in light reactions of photosynthesis for energy production and photoprotection. *J Exp Bot* **56**: 395–406

- Cruz JA, Sacksteder CA, Kanazawa A, Kramer DM (2001) Contribution of electric field ($\Delta\psi$) to steady-state thylakoid proton motive force (pmf) in vitro and in vivo: control of pmf parsing into $\Delta\psi$ and ΔpH by ionic strength. *Biochemistry* **40**: 1226–1237
- Damkjaer JT, Kereïche S, Johnson MP, Kovacs L, Kiss AZ, Boekema EJ, Ruban AV, Horton P, Jansson S (2009) The photosystem II light-harvesting protein Lhcb3 affects the macrostructure of photosystem II and the rate of state transitions in *Arabidopsis*. *Plant Cell* **21**: 3245–3256
- Duysens LNM, Sweers HE (1963) Mechanism of two photochemical reactions in algae as studied by means of fluorescence. In *Studies on Microalgae and Photosynthetic Bacteria*. University of Tokyo Press, Tokyo, pp 353–372
- Franck F, Juneau P, Popovic R (2002) Resolution of the photosystem I and photosystem II contributions to chlorophyll fluorescence of intact leaves at room temperature. *Biochim Biophys Acta* **1556**: 239–246
- Frydenvang J, van Maarschalkerweerd M, Carstensen A, Mundus S, Schmidt SB, Pedas PR, Laursen KH, Schjoerring JK, Husted S (2015) Sensitive detection of phosphorus deficiency in plants using chlorophyll *a* fluorescence. *Plant Physiol* **169**: 353–361
- Gilbert N (2009) The disappearing nutrient. *Nature* **461**: 716–718
- Goltsev VN, Kalaji HM, Paunov M, Bağa W, Horaczek T, Mojski J, Kociel H, Allakhverdiev SI (2016) Variable chlorophyll fluorescence and its use for assessing physiological condition of plant photosynthetic apparatus. *Russ J Plant Physiol* **63**: 869–893
- Grennan AK, Ort DR (2011) Measurement of chloroplast ATP synthesis activity in *Arabidopsis*. In PR Jarvis, ed, *Chloroplast Research in Arabidopsis*, Vol II. Humana Press, Totowa, NJ, pp 343–355
- Guo B, Jin Y, Wussler C, Blancaflor EB, Motes CM, Versaw WK (2008) Functional analysis of the *Arabidopsis* PHT4 family of intracellular phosphate transporters. *New Phytol* **177**: 889–898
- Hammond JP, White PJ (2008) Sucrose transport in the phloem: integrating root responses to phosphorus starvation. *J Exp Bot* **59**: 93–109
- Hawkesford M, Parmar S, Buchner P (2013) Mineral composition analysis: measuring anion uptake and anion concentrations in plant tissues. In JM Walker, ed, *Plant Mineral Nutrition*. Humana Press, York, UK, pp 109–119
- Heldt HW, Chon CJ, Maronde D, Herold A, Stankovic ZS, Walker DA, Kraminer A, Kirk MR, Heber U (1977) Role of orthophosphate and other factors in the regulation of starch formation in leaves and isolated chloroplasts. *Plant Physiol* **59**: 1146–1155
- Ihnatowicz A, Pesaresi P, Leister D (2007) The E subunit of photosystem I is not essential for linear electron flow and photoautotrophic growth in *Arabidopsis thaliana*. *Planta* **226**: 889–895
- Ihnatowicz A, Pesaresi P, Varotto C, Richly E, Schneider A, Jahns P, Salamini F, Leister D (2004) Mutants for photosystem I subunit D of *Arabidopsis thaliana*: effects on photosynthesis, photosystem I stability and expression of nuclear genes for chloroplast functions. *Plant J* **37**: 839–852
- Karlsson PM, Herdean A, Adolfsen L, Beebo A, Nziengui H, Irigoyen S, Ünneper R, Zsiros O, Garab G, Aronsson H, et al (2015) The *Arabidopsis* thylakoid transporter PHT4;1 influences phosphate availability for ATP synthesis and plant growth. *Plant J* **84**: 99–110
- Lauer MJ, Pallardy SG, Blevins DG, Randall DD (1989) Whole leaf carbon exchange characteristics of phosphate deficient soybeans (*Glycine max* L.). *Plant Physiol* **91**: 848–854
- Lavorel J, Etienne AL (1977) In vivo chlorophyll fluorescence. In J Barber, ed, *Primary Processes of Photosynthesis*. Elsevier, Amsterdam, pp 203–268
- Lunde C, Jensen PE, Haldrup A, Knoetzel J, Scheller HV (2000) The PSI-H subunit of photosystem I is essential for state transitions in plant photosynthesis. *Nature* **408**: 613–615
- MacDonald GK, Bennett EM, Potter PA, Ramankutty N (2011) Agronomic phosphorus imbalances across the world's croplands. *Proc Natl Acad Sci USA* **108**: 3086–3091
- Mimura T, Dietz KJ, Kaiser W, Schramm MJ, Kaiser G, Heber U (1990) Phosphate transport across biomembranes and cytosolic phosphate homeostasis in barley leaves. *Planta* **180**: 139–146
- Młodzińska E, Zboińska M (2016) Phosphate uptake and allocation: a closer look at *Arabidopsis thaliana* L. and *Oryza sativa* L. *Front Plant Sci* **7**: 1198
- Müller P, Li XP, Niyogi KK (2001) Non-photochemical quenching: a response to excess light energy. *Plant Physiol* **125**: 1558–1566
- Muneer S, Jeong BR (2015) Proteomic analysis provides new insights in phosphorus homeostasis subjected to Pi (inorganic phosphate) starvation in tomato plants (*Solanum lycopersicum* L.). *PLoS ONE* **10**: e0134103
- Pavón LR, Lundh F, Lundin B, Mishra A, Persson BL, Spetea C (2008) *Arabidopsis* ANTR1 is a thylakoid Na⁺-dependent phosphate transporter: functional characterization in *Escherichia coli*. *J Biol Chem* **283**: 13520–13527
- Porra RJ, Thompson WA, Kriedemann PE (1989) Determination of accurate extinction coefficients and simultaneous equations for assaying chlorophylls a and b extracted with four different solvents: verification of the concentration of chlorophyll standards by atomic absorption spectroscopy. *Biochim Biophys Acta* **975**: 384–394
- Queval G, Noctor G (2007) A plate reader method for the measurement of NAD, NADP, glutathione, and ascorbate in tissue extracts: application to redox profiling during *Arabidopsis* rosette development. *Anal Biochem* **363**: 58–69
- Ramaekers L, Remans R, Rao IM, Blair MW, Vanderleyden J (2010) Strategies for improving phosphorus acquisition efficiency of crop plants. *Field Crops Res* **117**: 169–176
- Rao IM, Terry N (1995) Leaf phosphate status, photosynthesis, and carbon partitioning in sugar beet. IV. Changes with time following increased supply of phosphate to low-phosphate plants. *Plant Physiol* **107**: 1313–1321
- Reich PB, Oleksyn J, Wright IJ (2009) Leaf phosphorus influences the photosynthesis-nitrogen relation: a cross-biome analysis of 314 species. *Oecologia* **160**: 207–212
- Reuter DJ, Robinson JB (1997) *Plant Analysis: An Interpretation Manual*, Ed 2. CSIRO Publishing, Collingwood, Australia
- Robinson C, Mant A (2002) *Molecular Plant Biology: A Practical Approach*. Oxford University Press, Oxford
- Robinson SP, Giersch C (1987) Inorganic phosphate concentration in the stroma of isolated chloroplasts and its influence on photosynthesis. *Aust J Plant Physiol* **14**: 451–462
- Ruban AV (2016) Nonphotochemical chlorophyll fluorescence quenching: mechanism and effectiveness in protecting plants from photodamage. *Plant Physiol* **170**: 1903–1916
- Rychter AM, Rao IM (2005) Role of phosphorus in photosynthetic carbon metabolism. In M Pessaraki, ed, *Handbook of Photosynthesis*, Ed 2. CRC Press, Boca Raton, FL, pp 123–148
- Schanker G, Tóth SZ, Strasser RJ (2005) Methylviologen and dibromothymoquinone treatments of pea leaves reveal the role of photosystem I in the Chl *a* fluorescence rise OJIP. *Biochim Biophys Acta* **1706**: 250–261
- Schlodder E, Meyer B (1987) pH dependence of oxygen evolution and reduction kinetics of photooxidized chlorophyll *a* (P-680) in photosystem II particles from *Synechococcus* sp. *Biochim Biophys Acta* **890**: 23–31
- Sharkey TD, Vanderveer PJ (1989) Stromal phosphate concentration is low during feedback limited photosynthesis. *Plant Physiol* **91**: 679–684
- Smith AM, Zeeman SC (2006) Quantification of starch in plant tissues. *Nat Protoc* **1**: 1342–1345
- Srivastava A, Strasser RJ, Govindjee (1995) Polyphasic rise of chlorophyll *a* fluorescence in herbicide-resistant D1 mutants of *Chlamydomonas reinhardtii*. *Photosynth Res* **43**: 131–141
- Stirbet A, Govindjee (2011) On the relation between the Kautsky effect (chlorophyll *a* fluorescence induction) and photosystem II: basics and applications of the OJIP fluorescence transient. *J Photochem Photobiol B* **104**: 236–257
- Stirbet A, Govindjee (2012) Chlorophyll *a* fluorescence induction: a personal perspective of the thermal phase, the J-I-P rise. *Photosynth Res* **113**: 15–61
- Stirbet A, Rznichenko GY, Rubin AB, Govindjee (2014) Modeling chlorophyll *a* fluorescence transient: relation to photosynthesis. *Biochemistry (Mosc)* **79**: 291–323
- Strand DD, Fisher N, Kramer DM (2017) The higher plant plastid NAD(P)H dehydrogenase-like complex (NDH) is a high efficiency proton pump that increases ATP production by cyclic electron flow. *J Biol Chem* **292**: 11850–11860
- Strand DD, Kramer DM (2014) Control of non-photochemical exciton quenching by the proton circuit of photosynthesis. In B Demmig-Adams, G Garab, W Adams, Govindjee, eds, *Non-photochemical Quenching and Energy Dissipation in Plants, Algae and Cyanobacteria*. Springer, Dordrecht, The Netherlands, pp 387–408
- Strasser RJ, Govindjee (1992) The Fo and the O-J-I-P fluorescence rise in higher plants and algae. In JH Argyroudi-Akoyunoglou, ed, *Regulation of Chloroplast Biogenesis*. Springer, Boston, pp 423–426
- Takizawa K, Kanazawa A, Kramer DM (2008) Depletion of stromal P(i) induces high 'energy-dependent' antenna exciton quenching (q(E)) by decreasing proton conductivity at CF(O)-CF(I) ATP synthase. *Plant Cell Environ* **31**: 235–243

- Tietz S, Hall CC, Cruz JA, Kramer DM** (2017) NPQ_(T): a chlorophyll fluorescence parameter for rapid estimation and imaging of non-photochemical quenching of excitons in photosystem-II-associated antenna complexes. *Plant Cell Environ* **40**: 1243–1255
- Tikhonov AN** (2013) pH-dependent regulation of electron transport and ATP synthesis in chloroplasts. *Photosynth Res* **116**: 511–534
- Tikhonov AN** (2014) The cytochrome b6f complex at the crossroad of photosynthetic electron transport pathways. *Plant Physiol Biochem* **81**: 163–183
- Tóth SZ, Schansker G, Strasser RJ** (2007) A non-invasive assay of the plastoquinone pool redox state based on the OJIP-transient. *Photosynth Res* **93**: 193–203
- Vredenberg WJ** (2004) System analysis and photoelectrochemical control of chlorophyll fluorescence in terms of trapping models of photosystem II: a challenging view. *In* GC Papageorgiou, Govindjee, eds, Chlorophyll a Fluorescence. Springer, Dordrecht, The Netherlands, pp 133–172
- Walan P, Davidsson S, Johansson S, Höök M** (2014) Phosphate rock production and depletion: regional disaggregated modeling and global implications. *Resour Conserv Recycling* **93**: 178–187
- Yan N, Zhang YL, Xue HM, Zhang XH, Wang ZD, Shi LY, Guo DP** (2015) Changes in plant growth and photosynthetic performance of *Zizania latifolia* exposed to different phosphorus concentrations under hydroponic condition. *Photosynthetica* **53**: 630–635
- Yin L, Vener AV, Spetea C** (2015) The membrane proteome of stroma thylakoids from *Arabidopsis thaliana* studied by successive in-solution and in-gel digestion. *Physiol Plant* **154**: 433–446
- Zhang K, Liu H, Tao P, Chen H** (2014) Comparative proteomic analyses provide new insights into low phosphorus stress responses in maize leaves. *PLoS ONE* **9**: e98215